Downscaling CESM2 in CLM5 to Hindcast Pre-Industrial Equilibrium Line Altitudes for Tropical Mountain Glaciers

Nicholas G. Heavens[1,2]

[1]Space Science Institute, 4765 Walnut St, Suite B, Boulder, CO 80301, USA
[2]Department of Earth Science and Engineering, Imperial College, London, United Kingdom

Key Points:

- Global model-forced standalone land model framework developed for simulating tropical mountain glaciation
- Equilibrium line altitude can be estimated with a bias of 249 ± 330 m where mountain peaks sufficiently resolved
- Bias comes from large-scale model precipitation and equilibrium line reconstruction uncertainties

Corresponding author: Nicholas G. Heavens, `nheavens@spacescience.org`

Abstract

Tropical mountain glaciers are an important water resource and highly impacted by recent climate change. Tropical mountain glaciation also occurred in the recent and deep past, which presents opportunities for better validating paleoclimate simulations in continental interiors and mountainous regions but requires bridging global model scales (100s of km) with the $\approx$ 1–10 km scale of glaciers when paleotopography is poorly known. Here we hindcast tropical mountain glaciation in pre-industrial time by using global climate model meteorology to force standalone simulations in its land component that use high resolution topography to resolve selected tropical mountain glaciers. These simulations underestimate observed equilibrium line altitudes (ELA) by 249 $\pm$ 330 m, but the simulated ELA and snow lines capture observed inter-mountain ELA variability. Error in large-scale model precipitation and ELA reconstruction uncertainty are the main contributors to this bias.

Plain Language Summary

Shrinking glaciers in mountains near the Equator are commonly used to illustrate present day climate change caused by greenhouse gas emissions from burning fossil fuels. These glaciers are not just picturesque but also can be an important source of water for humans. Geologists have found the traces of larger, lower elevation glaciers from the most recent ice ages and hundreds of millions of years ago. Global climate models can be used to assemble the characteristics of glaciers and other clues into an accurate picture of past climate, but global models consider what is happening at scales much bigger than glaciers. We wanted to predict how low glaciers reach in elevation in a particular global climate model experiment. We do this by taking the weather from the global model and putting it into a model that looks at processes similar in scale to glaciers. Our method underestimated glacier elevation but did get right how glacier elevation varied from mountain to mountain. Underestimating glacier elevation mainly resulting from overestimating precipitation in the global model and possible errors in our knowledge of past glaciers. This technique can be used to understand past climates, particularly if we have independent information about precipitation near glaciers.

1 Introduction

Tropical mountain glaciers can be a striking part of the landscape, because their high reflectivity at all visible wavelengths and very nature as frozen water can starkly contrast with the red, brown, and green colors and warmer and/or drier climates at nearby lower elevations. Shrinking tropical mountain glaciers in the industrial era have been used to illustrate how anthropogenic climate change has affected an aesthetically compelling feature of the environment (e.g., Mote & Kaser, 2007; Thompson et al., 2011). But the shrinking of these glaciers has more practical consequences for those who depend on them for fresh water or other climate services, principally in the Andes (e.g., Vuille et al., 2008; Mölg et al., 2008; Drenkhan et al., 2015)

Tropical mountain glaciers make such a good and potentially misleading (see Mote & Kaser, 2007) illustration of anthropogenic climate change, because they are highly sensitive to changes in temperature and precipitation. The equilibrium line altitude (ELA), the elevation at which long-term accumulation and ablation of ice balances, was typically $\approx$ 1 km lower at the Last Glacial Maximum (LGM) than around 1850 CE (Porter, 2001; Hastenrath, 2009). This change coincided with a 2–4 K change in tropical mean temperatures (Annan & Hargreaves, 2013), which was likely larger on mountains due to steeper lapse rates (Tripati et al., 2014; Loomis et al., 2017).

The ELA is a global property of a glacier. In areas with steeper slopes, glaciers can flow quite deeply into valleys, emplacing terminal moraines at elevations > 1 km below

the ELA that is rigorously obtained by calculating the mean elevation of the entire margin of the glacial front (Osmaston, 2004) and less rigorously by averaging the top and bottom elevation of the glacier (Porter, 2001).

Mountain glaciers' high climate sensitivity makes them potentially useful for validating paleoclimate simulations. The LGM is an obvious opportunity; sea surface temperature proxies are the gold standard for validation (e.g., Tierney et al., 2020), but mountain glacier properties are one of many ways simulations might be validated at higher elevations and continental interiors (e.g., Capron et al., 2019).

Tropical mountain glaciers also could provide similar insight into deep time climates. Glaciation in tropical highland environments is recorded in Late Carboniferous strata (300 Ma) in both France and Colorado (e.g., Julien, 1895; Soreghan et al., 2014; Pfeifer et al., 2021, and references therein). These Carboniferous deposits seem to record terminal moraines at altitudes < 2000 m, suggesting ELA was at least similar to the LGM (Soreghan et al., 2014).

However, global climate model (GCM) simulations using appropriate paleogeography and plausible greenhouse gas levels have been unable to reproduce stable glaciation at these elevations (Soreghan et al., 2008; Heavens et al., 2015), possibly they under-resolve glacial processes; even pre-industrial tropical glaciers typically were << 10 km in diameter (Kaser, 1999), which is small compared to the typical 200–400 km resolution of deep time climate model simulations. Deep time GCMs generally predict snow-fall and have been coupled with models that simulate ice sheets (e.g., Hyde et al., 2000; Poulsen et al., 2007; Horton et al., 2012), but prognostic climate simulations of mountain glaciation are relatively rare and require some form of downscaling from global GCM resolution (e.g., Kotlarski et al., 2010; Shannon et al., 2019).

Recently, a prognostic ice sheet model, the Community Ice System Model (CISM), was added as a fully coupled component to the Community Earth System Model (CESM) (Lipscomb et al., 2019). CISM takes ice mass balance information from the Community Land Model (CLM), which CLM predicts on the basis of atmospheric component (Community Atmosphere Model: CAM) temperature and precipitation information downscaled into multiple elevation classes of potential glaciers. Thus, the ice mass balance of a large grid cell is considered at an elevation around 3000 m, 2500 m, etc. according to model settings. CISM then translates that ice mass balance onto a grid with resolution as fine as 4 km and simulates ice flow. CLM version 5 (CLM5) was specifically modified to improve representation of processes related to hydrology, snowfall, and ice mass balance (Lawrence et al., 2019). But CLM5 (with or without CISM) was not designed to simulate mountain glaciation realistically because of concerns that under-resolving topography within the atmosphere model results in excessively warm climate and excessive runoff (UCAR, n.d.).

In this study, we demonstrate that CLM5's ice surface mass balance (SMB) capabilities can be successfully adapted to simulate tropical mountain glaciation in pre-industrial time: a necessary preliminary for validating global paleoclimate model simulations against tropical mountain glaciation information. Trying to connect global climate change quantitatively with the response of tropical mountain glaciation is nothing new (see Mölg and Kaser (2011); Roe et al. (2021) and references therein). The unique feature of this study is modeling tropical mountain glaciation entirely within the framework of a latest generation global climate model and its land component.

2 Methods

2.1 CESM2 and CLM5 Simulations

We performed standalone CLM5 simulations forced by a data atmosphere generated by a standard CESM2 simulation on the National Center for Atmospheric Research (NCAR) supercomputer Cheyenne (CISL, 2019). Because this is a non-standard configuration of CLM5, we have archived example case directories, configuration procedure documentation, and input files for these simulations within the data archive associated with this study (Heavens, 2021). Except for some simulations described later, the CLM5 code was modified to remove a step in the downscaling of downward longwave radiation at the surface (FLDS) that re-normalized the downscaled radiation fields between elevation classes. This change is consistent with each point in the land model being treated as a single elevation class and reduces mountain summit FLDS by $\approx 100 \ \mathrm{Wm^{-2}}$.

The CESM2 data atmosphere came from 30 years of a branch simulation from year 1101 of the Climate Model Intercomparison Project 6 (CMIP6) standard pre-industrial control for CESM2 at f09_g17 resolution ($0.9° \times 1.25°$) (Danabasoglu et al., 2020). A pre-industrial control simulation is perpetually forced by greenhouse gas levels for the year 1850 CE and is intended to reproduce long-term average climate prior to industrialization (Eyring et al., 2016). Standalone CLM5 simulations then were run in 11 limited area domains roughly centered on past or presently glaciated tropical mountains with well-documented ELA estimates (Table 1). Two domains with LGM mountain glaciation but no pre-industrial mountain glaciation (Table 1) were simulated to make sure ELA was not substantially underestimated in pre-industrial climate and to set a baseline for a future study of LGM climate. The selected areas cover a meridional transect in the tropics of Central and South America as well as a few domains in Africa and the Maritime Continent to cover a range of observed ELA and proximity to the ocean. This choice of domains is meant to span the potential range of precipitation, though this choice cannot be rigorous because of the sparseness of precipitation measurements and the heterogeneity of precipitation in these areas (e.g., La Frenierre & Mark, 2017).

Each domain was 2° in latitude and 1° in longitude. The selected domain size ensured multiple glaciated mountains and topography < 2000 m could be included in the domain (except in the High Andes). The domain is similar in size to 1–2 global model grid cells in the CESM2 simulation.

Each CLM5 simulation was initialized from high-resolution surface data and land domain files (nominally 100 points per degree) in which the global model resolution land surface properties except topography/slope were translated to the high-resolution domain by nearest neighbor interpolation. High resolution topography, standard deviation of elevation, and slope data were then added using 30 arc-second resolution data from GMTED2010 (Danielson & Gesch, n.d.). (Fig. 1a). The topography was used to assign each grid point to one of 10 possible elevation classes and set its elevation. To ensure SMB could be calculated, glacial column coverage was set to a minimum of 1% (or greater where the original land surface dataset had greater glacial column coverage). This additional glacial column coverage replaced coverage by vegetation. Glacier region was set to 2 (Greenland). We have verified by appropriate simulations that using the different elevation class treatments available for glacier regions 2 and 3 (Antarctica) or using 50% glacial coverage does not affect the results of this type of simulation as long as the SMB and related calculations are analyzed on the glaciated land units alone. In effect, these experiments impose a glacier of 50 m altitude (as evident from the documentation and initial grid cell ice content variable, ICE_CONTENT1) over a limited grid cell area, in circumstances where glaciation has no or minimal impact on large-scale climate, and simulate how it accumulates or ablates over a climatological normal period.

Table 1. High resolution domains used for standalone CLM5 simulations. Most features listed and ELA values come from Porter (2001) and Hastenrath (2009). ELA for Puncak Jaya (Permana, 2011; Permana et al., 2019) is extrapolated from 1972 to 1850 based on Allison and Kruss (1977). Distance from the ocean was calculated using the distance calculator in Google Earth and is listed with a 5 km precision.

Number	Latitude Bounds (°N)	Longitude Bounds (°E)	Mountains/ Features	Est. Pre-Industrial ELA (m)	Minimum Distance from Ocean (km)
1	18.5, 20.5	-99.5, -98.5	Iztaccihuatl, Mexico	4880	225
2	8.5, 10.5	-84,-83	Cherro Chirripo, Costa Rica	>3819	50
3	4,6	-76,-75	Los Nevados de Santa Isabel y del Ruiz, Colombia	4750, 4850	220, 235
4	-2, 0	-79,-78	Chimborazo+ Antisana, Ecuador	4715, 4850	210, 215
5	-10,-8	-78,-77	Huascaran, Peru	5000	95
6	-18.5,-16.5	-69.85,-68.85	Nevado Sajama, Bolivia; Parinacota, Chile	5550, 5600	160, 115
7	-1,1	37,38	Mt. Kenya, Kenya	4712.5	440
8	-4,-2	37,38	Mt. Kilimanjaro, Tanzania (Kibo and Mawenzi peaks)	5030, 5407.5	285
9	-1,1	29.5,30.5	Mt. Ngaliema, Uganda	4495	1205
10	5,7	116,117	Kinabalu, Malaysia	>4095	40
11	-4.9,-2.9	136.7,137.7	Puncak Jaya, Indonesia	4482	100

The experiments were cold started (because only physical climate was of interest) and used crop-biogeochemistry physics routines, because agricultural activity occurs in some of the domains and it was therefore necessary to include crop biomes. Lapse rate was set to the mean free air temperature lapse rate for the domain derived from the CESM2 simulation. FLDS lapse rate was set to the standard CLM5 setting of 0.032 Wm^{-2} m^{-1} (Van Tricht et al., 2016; Lawrence et al., 2019). (Positive lapse rate is defined here as decreasing with height.)

The mean free air lapse rate in each CLM5 domain was calculated by calculating the mean lapse rate in the troposphere as defined by WMO (1957) for every grid point of each monthly mean output file of the CESM2 simulation, interpolating this onto each CLM5 domain in the same way as the CLM5 boundary condition files, and then averaging over 30 years. The results in all cases are between 6 and 7 K km^{-1} (Table 2).

To test sensitivity to FLDS, two simulations were performed in domain 4 (Table 1) with lapse rates of 6 and 7 K km^{-1} without modifying the FLDS downscaling in CLM5. Two additional simulations in domain 4 were performed with the FLDS downscaling modified and temperature lapse rates of 7 K km^{-1} and 4.5 K km^{-1} to span the reported mean lapse rates for proximal areas of the Andes (Córdova et al., 2016; Navarro-Serrano et al., 2020).

2.2 Analysis

The results of each simulation then were analyzed to extract ELA and ELA-related metrics. ELA, strictly speaking, is the elevation where ablation and accumulation are in balance, that is, where long-term SMB is equal to zero. Following Vizcaíno et al. (2014),

$$SMB = SNOW + RAIN - RUNOFF - SUBLIMATION \tag{1}$$

This balance can be expressed in CLM5 output variables restricted to glaciated land units only.

$$SMB = SNOW\_ICE + RAIN\_ICE - QRUNOFF\_ICE - QFLX\_SUB\_SNOW\_ICE \tag{2}$$

where the quantities in brackets correspond to the terms of Eq. 1 and SNOW_ICE, RAIN_ICE, QRUNOFF_ICE, and QFLX_SUB_SNOW_ICE are variables output by CLM5. From this point onward, we will use SMB to mean the integrated SMB over the 30 year period of each simulation (Fig. 1b).

The mean annual precipitation for each domain coming from the data atmosphere was calculated by calculating the 30 year mean of (RAIN_FROM_ATM+SNOW_FROM_ATM). We also estimated a freezing zone elevation by taking the 30 year mean of the downscaled 2 m air temperature variable over ice, TSA_ICE and calculating the minimum elevation where this mean was < 273.15 K.

ELA in the absence of flow (ELA$_{noflow}$) was estimated by dividing the domain into connected regions with SMB > 0. ELA then was defined as the minimum altitude of each region. By determining the maximum altitude of each region, it was possible to assign each region to a mountain with observed ELA estimates. In some cases, however, two mountain peaks with estimates were in the same connected region.

An ELA metric accounting for flow (ELA$_{flow}$) was calculated by first estimating the minimum possible elevation of a terminal moraine originating from each connected regions with SMB > 0. The product of SMB and area for each connected region as well as the path with steepest slope connected to the maximum altitude of the region were

determined. The product of SMB and area in the ablation region along this path were
integrated and subtracted from the sum of SMB and area in the accumulation zone formed
by the connected regions. This is equivalent to determining how low in elevation could
the accumulated ice go if ice were continuously delivered along a one grid cell wide val-
ley originating from the region. ELA_{flow} then was estimated as the average of the peak
altitude of the region and the elevation of the terminal moraine in line with a typical tech-
nique for estimating ELA in the field (Porter, 2001). This type of calculation is illustrated
in Figs. 1c–d.

The snow line has been used to approximate ELA under some circumstances (Porter,
2001). So for comparison, two estimates of the permanent snow line also were calculated.
SL and SL_{1m} were defined as the minimum altitude at which snow and snow of 1 m depth
were present in each month during the last month of the simulation, respectively. These
metrics were calculated for the whole domain by averaging the minimum elevation where
snow is present and the maximum elevation where snow is absent by analogy with the
glaciation-threshold method (Porter, 2001). In each case, snow depth was normalized
by the fraction of glacial coverage to obtain the true snow depth in the glacial column.
Note that SL_{1m} tends to highlight a small range of elevation where snow depth rapidly
increases: a true snow line. Thus, choosing a much higher depth criterion only would marginally
change ELA. In one simulation, SL_{1m} is 4362 m, but SL_{10m} is only 4405 m (Fig. S1).

3 Results

The results of this analysis are given in Table 2. The non-glaciated mountains of
Ajusco, Cerro Chrirripo, and Kinabalu all are hindcast as non-glaciated. However, the
simulations also hindcast Mts. Kenya and Ngaliema as being non-glaciated. This is most
likely a resolution problem. For Mt. Ngaliema, uncertainty in the observed ELA is large
and the upper bound of ELA it implies is greater than the height of Mt. Ngaliema re-
solved by the model (Table 2). For Mt. Kenya, the observed ELA is within 100 m of the
model-resolved height (Table 2). The model domains do not resolve the highest peaks
in several other cases, but the highest elevation in the model is typically significantly greater
than the ELA. A similar resolution problem makes it difficult to resolve Kilimanjaro's
Kibo and Mawenzi peaks, so Kibo peak only will be considered in the remainder of the
analysis.

For ten sufficiently resolved mountains with observed glaciation, the bias (Δ) in
the simulated ELA for each of the metrics was estimated by taking the mean and stan-
dard deviation of the difference between the estimated and observed ELA (Fig. S2). ELA_{noflow}
underestimates observed ELA by 249 ± 330 m. Accounting for flow (ELA_{flow}) reduces
the underestimate to 235 m but greatly widens the uncertainty. But as noted by Porter
(2001), the method used to derive ELA from terminal moraine elevation may overesti-
mate ELA by up to 150 m, making ELA_{flow} no superior to that derived based on SMB
alone. The average simulated snow line is 1084 m below the observed ELA. However,
requiring 1 m of permanent snow depth reduces this underestimate to 324 m with com-
parable uncertainty to ELA, suggesting that the snow line illustrated in Fig. S1 is a good
approximation to ELA rather than a snow line based on a minimal amount of snow. The
magnitude and variability of biases in all ELA metrics are large enough that they ex-
ceed the largest reported uncertainties in observed ELA.

The simulated ELA metrics follow the variability in observed ELA (Fig. S2). Higher
observed ELA usually results in higher simulated ELA, suggesting that the simulated
ELA is capturing the variability in observed ELA but underestimating its magnitude.
For example, the correlation between ELA_{noflow} and SL_{1m} and observed ELA is r=0.94
and r=0.94 respectively (n=10), which is significant to p<0.001. This correlation is weaker
for the other metrics but is still significant to p<0.01. Because of its intuitiveness and
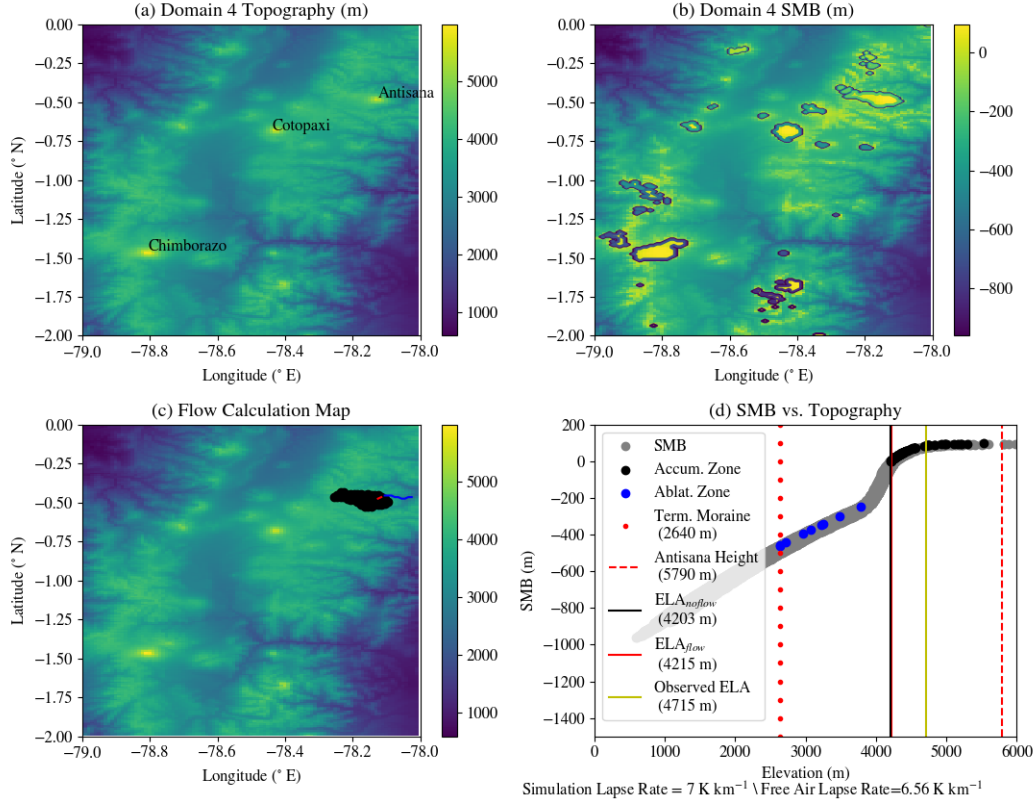correlation with observed ELA, we consider ELA_{noflow} to be the most useful ELA met-

Figure 1. Example CLM5 standalone simulation and its analysis, as labeled: (a) Topographic grid (m). Mountains of interest are labeled, but only Chimborazo and Antisana have ELA estimates; (b) Net SMB for the simulation (m). Connected regions (accumulation zones) are indicated by contours; (c) Topographic map (m) showing the accumulation zone for Antisana in black and the steepest path from the peak used to find the minimum elevation for a terminal moraine in blue; (d) SMB vs. topography for the entire domain with relevant estimates and observations for Antisana labeled.

ric, and we will focus on attribution of its bias in the remainder of this study. Global variability in ELA_{noflow} is explained by precipitation coming from the GCM, with which it is strongly correlated (r=-0.91, p<0.001) (Fig. 2a). This strong relationship between precipitation and ELA_{noflow} contrasts with the insignificant correlation between ELA_{noflow} and freezing zone elevation (r= 0.12) and the narrow range in freezing zone elevation (Fig. S3). Modeled air temperatures can average below freezing > 1000 m below the hindcast ELA_{noflow} (Fig. S3).

Two possible sources of bias in ELA are the major free parameters of the experiments, the temperature and FLDS lapse rates, particularly in domain 4. We first consider temperature lapse rate. In domain 4, ELA is underestimated by $\sim$ 400 m (Table 2). Estimates of the mean near-surface lapse rate over the Andes in or near domain 4 vary from $\sim$ 4.5–6.9 K km^{-1} (Córdova et al., 2016; Navarro-Serrano et al., 2020) (a much larger range than would be expected for the change in free air lapse rate between 1850 and the present day), which would be consistent with ELA_{noflow} of 4288–5178 m for Chimborazo and 4237–5161 m on Antisana (Table 2). Thus, the gentler lapse rates of Córdova et al. (2016) would explain 778 m of bias, (173% of the total) at Chimborazo, and 810 m (225% of the total) at Antisana.

Despite being derived from observations over Greenland (Van Tricht et al., 2016), the FLDS lapse rate agrees well with available observations in domain 4. Annual mean FLDS on Antisana was 283 Wm^{-2} during 2005–2006 (Wagnon et al., 2009). We used the assumed FLDS lapse rate to translate between the elevation of these observations and the elevation of the nearest grid point in the high resolution grid ($\sim$ 300 m). We then compared the annual mean FLDS at the nearest grid point in the CESM2 simulation with the annual mean FLDS for the period sampled by Wagnon et al. (2009) in the CESM2 CMIP6 historical simulation (b.e21.BHIST.f09_g17.CMIP6-historical.003) at the same grid point. This comparison implies FLDS was 1.4 Wm^{-2} greater during 2005–2006 than around 1850. With all of these adjustments made, the expected annual mean FLDS in standalone CLM5 simulations at Wagnon et al. (2009)'s observation site on Antisana should be 275 Wm^{-2}, 8 Wm^{-2} lower than observed. This is equivalent to a +8% error in the assumed FLDS lapse rate. If the standard CLM5 downscaling is used, the annual mean FLDS is 381.41 Wm^{-2}. At a temperature lapse rate of 7 K km^{-1}, the sensitivity in ELA_{noflow} to FLDS is 9.2 m (Wm^{-2})$^{-1}$, explaining an ELA_{noflow} underestimate of 77 m, 21% of ΔELA_{noflow} at Antisana. (Interpolating the results of the standard CLM5 downscaling simulations to 6.56 K km^{-1} and differencing with the 6.56 K km^{-1} lapse rate modified downscaling simulation for domain 4 only changes this result to 87 m and 24%).

Another possible source of bias is data atmosphere precipitation bias. Meteorological observations from the Quito Observatory in domain 4 start from 1894 and suggest mean annual precipitation for pre-industrial climate was 1000 mm (Domínguez-Castro et al., 2018), $\sim$ 2200 mm less than provided by the data atmosphere and equivalent to 66 m of SMB. If this excess SMB is removed from the domain 4 simulation and re-analyzed, ELA_{noflow} increases to 4760 m (+360 m, 80% of the bias) on Chimborazo and 4680 m (+329 m, 90% of the bias) on Antisana (Fig. 2b).

4 Discussion

Where it resolves glaciers, our hindcasting framework typically underestimates ELA, naively implying a cold bias in simulating tropical mountain climates. This result is somewhat surprising in light of the concern of (UCAR, n.d.) that CLM5 mountain glaciation simulations would be biased warm. However, hindcast ELA in the tropics seems largely controlled by precipitation rather than temperature (Figs. 2a-b; S3). Mean air temperatures are generally below freezing above 4100 m elevation, but substantial precipitation (ideally snowfall, which does not immediately contribute to runoff) is required to

Table 2. Results of the CLM5 standalone simulations for each mountain of interest. Ice-free and snow-free indicate where glaciation is not observed or ELA cannot be defined, MWHP indicates merger of glaciation of that mountain with a higher peak. Italicized mountain names indicate simulations and mountains used to estimate bias in simulated ELA. ELA data come from Porter (2001) and Hastenrath (2009)

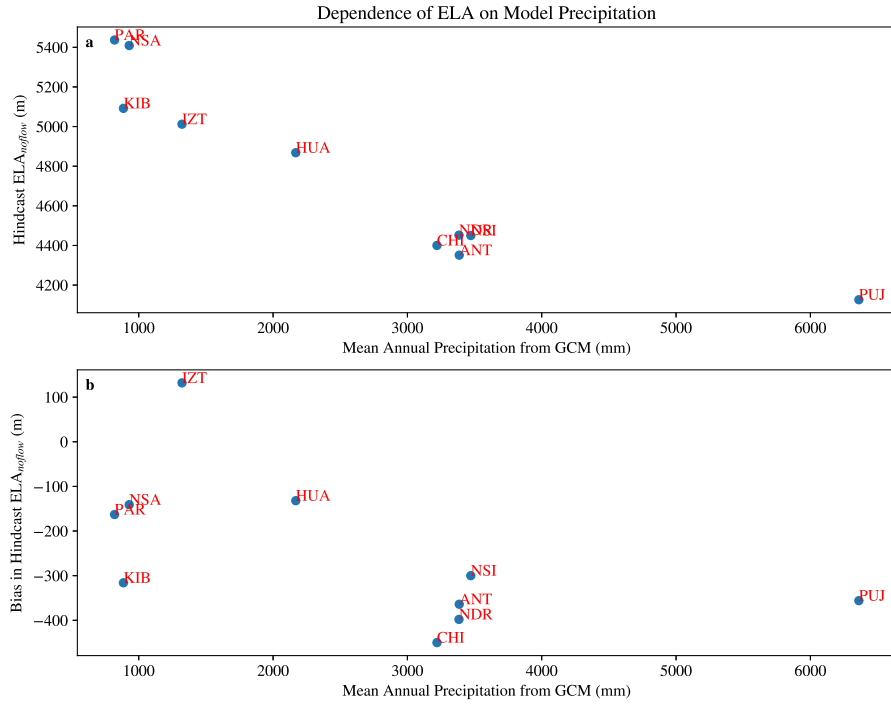| Mountain	Domain Lapse Rate (K/km)	Longwave Downscaling	Height (m)	Height in Model (m)	Obs. ELA (m)	ELA_{noflow} (m)	ELA_{flow} (m)	SL (m)	SL_{1m} (m)
Iztaccihuatl (IZT)	6.39	Modified	5286	5012	4880	5012	5148	3783	4865
Ajusco	6.39	Modified	3937	3720	Ice-free	Ice-free	Ice-free	3826	Snow-free
Cerro Chirripo	6.45	Modified	3819	3656	Ice-free	Ice-free	Ice-free	Snow-free	Snow-free
Chimborazo (CHI)	6.56	Modified	6310	5983	4850±50	4400	4826	3861	4362
Chimborazo	7	CLM5 Standard	6310	5983	4850±50	5072	5356	3971	5039
Chimborazo	6	CLM5 Standard	6310	5983	4850±50	5811	5905	4379	5703
Chimborazo	4.5	Modified	6310	5983	4850±50	5178	5370	4939	5148
Chimborazo	7	Modified	6310	5983	4850±50	4255	4826	3729	4217
Antisana (ANT)	6.56	Modified	5790	5529	4715±115	4351	4371	3861	4362
Antisana	7	CLM5 Standard	5790	5529	4715±115	5105	5191	3971	5039
Antisana	6	CLM5 Standard	5790	5529	4715±115	Ice-free	Ice-free	4379	5703
Antisana	4.5	Modified	5790	5529	4715±115	5161	5414	4939	5148
Antisana	7	Modified	5790	5529	4715±115	4203	4215	3729	4217
Huascaran (HUA)	6.65	Modified	6768	6293	5000	4868	5349	4079	4825
Nevado de Santa Isabel (NSI)	6.56	Modified	4950	4814	4750	4450	4448	3849	4296
Nevado del Ruiz (NDR)	6.56	Modified	5321	5215	4850	4452	4402	3849	4296
Parinacota (PAR)	6.8	Modified	6348	6240	5600	5437	5048	4311	5356
Nevado Sajama (NSJ)	6.8	Modified	6542	6240	5550±150	5409	5831	4311	5356
Mt. Ngaliema	6.59	Modified	5109	4670	4495±225	Ice-free	Ice-free	3812	Snow-free
Mt. Kenya	6.54	Modified	5202	4839	4712.5±12.5	Ice-free	Ice-free	4023	Snow-free
Mawenzi (Kilimanjaro)	6.45	Modified	5147	blends with Kibo	5030	MWHP	MWHP	3944	5021
Kibo (Kilimanjaro) (KIB)	6.45	Modified	5895	5794	5408±47.5	5092	5096	3944	5021
~~Kinabalu~~ Kinabalu	6.66	Modified	4095	3985	Ice-free	Ice-free	Ice-free	3897	Snow-free
Puncak Jaya (PUJ)	6.69	Modified	4884	4946	4482	4126	3220	3685	4111

Figure 2. (a) ELA_{noflow} (m) vs. precipitation coming from the data atmosphere (mm); (b) Bias in ELA_{noflow} (m) vs. precipitation coming from the data atmosphere (mm); The abbreviations used are given in Table 2.

outpace melting and sublimation due to absorption of shortwave and longwave radiation as well as temperatures rising above freezing seasonally.

Thus, ELA bias either could be entirely explained by the wide possible difference between near-surface temperature lapse rate and free air lapse rate, or by excess precipitation coming from CESM2. But the strong dependence of hindcast ELA on precipitation suggests the latter is more likely. Moreover, lapse rate bias would explain too much of the ELA bias, requiring some other compensating factor to be invoked. Using near-surface lapse rate information in CLM5 probably would be the correct protocol if precipitation type strongly depended on near-surface air temperature, but precipitation type is initially set by cloud temperature, which may be better extrapolated from the free air lapse rate. CESM2 is considered highly skillful among CMIP6 models in simulating precipitation in the tropical Andes, but still seems to have significant bias locally (Almazroui et al., 2021). In some cases, ELA bias cannot be easily attributed to precipitation bias. Precipitation at Iztaccihuatl (Fig. 2a) is realistic or slightly excessive for the area around Mexico City (Lemos-Espinal & Ballinger, 1995), but there is a positive bias in ELA of ~ 100 m (Fig. 2b). Biases of this magnitude may come from ELA reconstruction uncertainty (including the possibility that the glaciers not being really at equilibrium) (Porter, 2001; Hastenrath, 2009). ELA uncertainty estimates for other peaks are up to ± 150 m (Table 2). Kibo has the opposite problem, a large negative bias in ELA at low mean annual precipitation (Fig. 2b). But, here, too, ELA reconstruction may be at issue. The adjoining Mawenzi Peak has an observed ELA of 5030 m (378 m below Kibo), which would explain 120% of the bias.

It thus appears that correcting for model precipitation and ELA uncertainty makes our hindcasting framework a success. However, while freezing zone elevation is probably relatively similar across the tropics for pre-industrial climate, it likely changes as global climate warms and cools, driving ELA change. Therefore, paleoclimate model validation experiments that use tropical mountain glacier information will have to rely on local precipitation proxy information to distinguish global-scale temperature bias from local precipitation bias.

5 Summary

In this study, we have shown how downscaling CESM2 global simulations in CLM5 can hindcast tropical mountain glaciation in pre-industrial climate. This technique may be broadly valuable for paleoclimate model validation for models analogous in capability to CESM2 and CLM5 for any period with identified tropical mountain glaciation. Note, however, that tropical mountain glaciation information should be interpreted in tandem with proximal, independent precipitation proxy data to avoid mistaking a local signal in precipitation for a global signal in temperature.

References

Allison, I., & Kruss, P. (1977). Estimation of recent climate change in irian jaya by numerical modeling of its tropical glaciers. *Arctic and Alpine Research*, *9*(1), 49. doi: 10.2307/1550408

Almazroui, M., Ashfaq, M., Islam, M. N., Rashid, I. U., Kamil, S., Abid, M. A., ... et al. (2021). Assessment of cmip6 performance and projected temperature

and precipitation changes over south america. *Earth Systems and Environment*, *5*(2), 155–183. doi: 10.1007/s41748-021-00233-6

Annan, J. D., & Hargreaves, J. C. (2013). A new global reconstruction of temperature changes at the last glacial maximum. *Climate of the Past*, *9*(1), 367–376. Retrieved from https://cp.copernicus.org/articles/9/367/2013/ doi: 10.5194/cp-9-367-2013

Capron, E., Rovere, A., Austermann, J., Axford, Y., Barlow, N. L., Carlson, A. E., ... Wolff, E. W. (2019). Challenges and research priorities to understand interactions between climate, ice sheets and global mean sea level during past interglacials. *Quaternary Science Reviews*, *219*, 308-311. Retrieved from https://www.sciencedirect.com/science/article/pii/S0277379119305207 doi: https://doi.org/10.1016/j.quascirev.2019.06.030

CISL. (2019). *Cheyenne: HPE/SGI ICE XA System (University Community Computing)*. Boulder, CO: National Center for Atmospheric Research. doi: 10.5065/D6RX99HX

Córdova, M., Célleri, R., Shellito, C. J., Orellana-Alvear, J., Abril, A., & Carrillo-Rojas, G. (2016). Near-Surface Air Temperature Lapse Rate Over Complex Terrain in the Southern Ecuadorian Andes: Implications for Temperature Mapping. *Arctic, Antarctic, and Alpine Research*, *48*(4), 673-684. Retrieved from https://doi.org/10.1657/AAAR0015-077 doi: 10.1657/AAAR0015-077

Danabasoglu, G., Lamarque, J.-F., Bacmeister, J., Bailey, D. A., DuVivier, A. K., Edwards, J., ... Strand, W. G. (2020). The Community Earth System Model Version 2 (CESM2). *Journal of Advances in Modeling Earth Systems*, *12*(2), e2019MS001916. Retrieved from https://agupubs.onlinelibrary.wiley.com/doi/abs/10.1029/2019MS001916 (e2019MS001916 2019MS001916) doi: https://doi.org/10.1029/2019MS001916

Danielson, J., & Gesch, D. (n.d.). *Global multi-resolution terrain elevation data 2010 (GMTED2010)* (No. 2011–1073). USGS Open File Report.

Domínguez-Castro, F., García-Herrera, R., & Vicente-Serrano, S. M. (2018). Wet and dry extremes in quito (ecuador) since the 17th century. *International Journal of Climatology*, *38*(4), 2006-2014. Retrieved from https://rmets.onlinelibrary.wiley.com/doi/abs/10.1002/joc.5312 doi: https://doi.org/10.1002/joc.5312

Drenkhan, F., Carey, M., Huggel, C., Seidel, J., & Oré, M. T. (2015). The changing water cycle: climatic and socioeconomic drivers of water-related changes in the Andes of Peru. *WIREs Water*, *2*(6), 715-733. Retrieved from https://onlinelibrary.wiley.com/doi/abs/10.1002/wat2.1105 doi: https://doi.org/10.1002/wat2.1105

Eyring, V., Bony, S., Meehl, G. A., Senior, C. A., Stevens, B., Stouffer, R. J., & Taylor, K. E. (2016). Overview of the coupled model intercomparison project phase 6 (cmip6) experimental design and organization. *Geoscientific Model Development*, *9*(5), 1937–1958. Retrieved from https://gmd.copernicus.org/articles/9/1937/2016/ doi: 10.5194/gmd-9-1937-2016

Hastenrath, S. (2009). Past glaciation in the tropics. *Quaternary Science Reviews*, *28*(9), 790-798. Retrieved from https://www.sciencedirect.com/science/article/pii/S0277379108003521 doi: https://doi.org/10.1016/j.quascirev.2008.12.004

Heavens, N. G. (2021). *CESM2-CLM5 Framework for Hindcasting Tropical Mountain Glaciation: Examples and Pre-Industrial Validation Analysis version 2*. Mendeley Data. doi: 10.17632/68cdfyssgs.2

Heavens, N. G., Mahowald, N. M., Soreghan, G. S., Soreghan, M. J., & Shields, C. A. (2015). A model-based evaluation of tropical climate in pangaea during the late palaeozoic icehouse. *Palaeogeography, Palaeoclimatology, Palaeoecology*, *425*, 109-127. Retrieved from https://www.sciencedirect.com/

science/article/pii/S0031018215000802 doi: https://doi.org/10.1016/
j.palaeo.2015.02.024

Horton, D. E., Poulsen, C. J., Montañez, I. P., & DiMichele, W. A. (2012).
Eccentricity-paced late Paleozoic climate change. *Palaeogeography, Palaeo-
climatology, Palaeoecology*, *331-332*, 150-161. Retrieved from https://
www.sciencedirect.com/science/article/pii/S003101821200154X doi:
https://doi.org/10.1016/j.palaeo.2012.03.014

Hyde, W. T., Crowley, T. J., Baum, S. K., & Peltier, W. R. (2000, May). Neopro-
terozoic 'snowball Earth' simulations with a coupled climate/ice-sheet model.
Nature, *405*(6785), 425–429. doi: 10.1038/35013005

Julien, A. (1895). Ancien glaciers de la période houillère dans le plateau central de
la France. *Ann. Club Alp. Fr.*, *21*, 1–28.

Kaser, G. (1999). A review of the modern fluctuations of tropical glaciers.
Global and Planetary Change, *22*(1), 93-103. Retrieved from https://
www.sciencedirect.com/science/article/pii/S0921818199000284 doi:
https://doi.org/10.1016/S0921-8181(99)00028-4

Kotlarski, S., Jacob, D., Podzun, R., & Paul, F. (2010, Jan). Representing glaciers
in a regional climate model. *Climate Dynamics*, *34*(1), 27–46. doi: 10.1007/
s00382-009-0685-6

La Frenierre, J., & Mark, B. G. (2017). Detecting Patterns of Climate Change at
Volcán Chimborazo, Ecuador, by Integrating Instrumental Data, Public Ob-
servations, and Glacier Change Analysis. *Annals of the American Association
of Geographers*, *107*(4), 979-997. Retrieved from https://doi.org/10.1080/
24694452.2016.1270185 doi: 10.1080/24694452.2016.1270185

Lawrence, D. M., Fisher, R. A., Koven, C. D., Oleson, K. W., Swenson, S. C.,
Bonan, G., ... Zeng, X. (2019). The Community Land Model Version 5:
Description of New Features, Benchmarking, and Impact of Forcing Uncer-
tainty. *Journal of Advances in Modeling Earth Systems*, *11*(12), 4245-4287.
Retrieved from https://agupubs.onlinelibrary.wiley.com/doi/abs/
10.1029/2018MS001583 doi: https://doi.org/10.1029/2018MS001583

Lemos-Espinal, J. A., & Ballinger, R. E. (1995). Comparative thermal ecology of the
high-altitude lizard sceloporus grammicus on the eastern slope of the iztaccihu-
atl volcano, puebla, mexico. *Canadian Journal of Zoology*, *73*(12), 2184–2191.
doi: 10.1139/z95-258

Lipscomb, W. H., Price, S. F., Hoffman, M. J., Leguy, G. R., Bennett, A. R.,
Bradley, S. L., ... Worley, P. H. (2019). Description and evaluation of the
community ice sheet model (cism) v2.1. *Geoscientific Model Development*,
12(1), 387–424. Retrieved from https://gmd.copernicus.org/articles/12/
387/2019/ doi: 10.5194/gmd-12-387-2019

Loomis, S. E., Russell, J. M., Verschuren, D., Morrill, C., De Cort, G., Sin-
ninghe Damsté, J. S., ... Kelly, M. A. (2017). The tropical lapse rate steep-
ened during the Last Glacial Maximum. *Science Advances*, *3*(1). Retrieved
from https://advances.sciencemag.org/content/3/1/e1600815 doi:
10.1126/sciadv.1600815

Mölg, T., Hardy, D. R., Cullen, N. J., & Kaser, G. (2008). Tropical Glaciers, Cli-
mate Change, and Society: focus on Kilimanjaro (East Africa). In *Darkening
peaks: glacier retreat, science, and society.* Berkeley: University of California
Press.

Mölg, T., & Kaser, G. (2011). A new approach to resolving climate-cryosphere
relations: Downscaling climate dynamics to glacier-scale mass and energy
balance without statistical scale linking. *Journal of Geophysical Research:
Atmospheres*, *116*(D16). Retrieved from https://agupubs.onlinelibrary
.wiley.com/doi/abs/10.1029/2011JD015669 doi: https://doi.org/10.1029/
2011JD015669

Mote, P., & Kaser, G. (2007). The Shrinking Glaciers of Kilimanjaro: Can Global

Warming Be Blamed? *American Scientist*, *95*(4), 318. doi: 10.1511/2007.66 .318

Navarro-Serrano, F., López-Moreno, J. I., Domínguez-Castro, F., Alonso-González, E., Azorin-Molina, C., El-Kenawy, A., & Vicente-Serrano, S. M. (2020). Maximum and minimum air temperature lapse rates in the andean region of ecuador and peru. *International Journal of Climatology*, *40*(14), 6150-6168. Retrieved from `https://rmets.onlinelibrary.wiley.com/doi/abs/10.1002/joc.6574` doi: https://doi.org/10.1002/joc.6574

NCAR. (2018). *b.e21.BHIST.f09_g17.CMIP6-historical.003 data.* Earth System Grid. Retrieved from `https://www.earthsystemgrid.org/dataset/ucar.cgd.cesm2.b.e21.BHIST.f09_g17.CMIP6-historical.003.html`

Osmaston, H. (2004). Quaternary glaciation in the East African mountains. In *Quaternary Glaciations - Extent and Chronology Part III: South America, Asia, Africa, Australia, Antarctica.* Amsterdam: Elsevier.

Permana, D. S. (2011). *Climate, ptrecipitation isotopic composition and tropical ice core analysis of papua, indonesia* (Unpublished master's thesis). The Ohio State University, `https://etd.ohiolink.edu/apexprod/rws_olink/r/1501/10?clear=10&p10_accession_num=osu1313480990`.

Permana, D. S., Thompson, L. G., Mosley-Thompson, E., Davis, M. E., Lin, P.-N., Nicolas, J. P., ... Mark, B. G. (2019). Disappearance of the last tropical glaciers in the western pacific warm pool (papua, indonesia) appears imminent. *Proceedings of the National Academy of Sciences*, *116*(52), 26382–26388. Retrieved from `https://www.pnas.org/content/116/52/26382` doi: 10.1073/pnas.1822037116

Pfeifer, L. S., Soreghan, G. S., Pochat, S., & Van Den Driessche, J. (2021, Jan). Loess in eastern equatorial pangea archives a dusty atmosphere and possible upland glaciation. *GSA Bulletin*, *133*(1–2), 379–392. doi: 10.1130/B35590.1

Porter, S. C. (2001). Snowline depression in the tropics during the last glaciation. *Quaternary Science Reviews*, *20*(10), 1067-1091. Retrieved from `https://www.sciencedirect.com/science/article/pii/S0277379100001785` doi: https://doi.org/10.1016/S0277-3791(00)00178-5

Poulsen, C. J., Pollard, D., Montañez, I. P., & Rowley, D. (2007). Late Paleozoic tropical climate response to Gondwanan deglaciation. *Geology*, *35*(9), 771. doi: 10.1130/G23841A.1

Roe, G. H., Christian, J. E., & Marzeion, B. (2021). On the attribution of industrial-era glacier mass loss to anthropogenic climate change. *The Cryosphere*, *15*(4), 1889–1905. Retrieved from `https://tc.copernicus.org/articles/15/1889/2021/` doi: 10.5194/tc-15-1889-2021

Shannon, S., Smith, R., Wiltshire, A., Payne, T., Huss, M., Betts, R., ... Harrison, S. (2019). Global glacier volume projections under high-end climate change scenarios. *The Cryosphere*, *13*(1), 325–350. Retrieved from `https://tc.copernicus.org/articles/13/325/2019/` doi: 10.5194/tc-13-325-2019

Soreghan, G. S., Soreghan, M. J., Poulsen, C. J., Young, R. A., Eble, C. F., Sweet, D. E., & Davogustto, O. C. (2008). Anomalous cold in the Pangaean tropics. *Geology*, *36*(8), 659. doi: 10.1130/G24822A.1

Soreghan, G. S., Sweet, D. E., & Heavens, N. G. (2014). Upland glaciation in tropical pangaea: Geologic evidence and implications for late paleozoic climate modeling. *The Journal of Geology*, *122*(2), 137-163. Retrieved from `https://doi.org/10.1086/675255` doi: 10.1086/675255

Thompson, L. G., Mosley-Thompson, E., Davis, M. E., & Brecher, H. H. (2011). Tropical glaciers, recorders and indicators of climate change, are disappearing globally. *Annals of Glaciology*, *52*(59), 23–34. doi: 10.3189/172756411799096231

Tierney, J. E., Zhu, J., King, J., Malevich, S. B., Hakim, G. J., & Poulsen, C. J. (2020). Glacial cooling and climate sensitivity revisited. *Nature*, *584*(7822),

569–573. doi: 10.1038/s41586-020-2617-x

Tripati, A. K., Sahany, S., Pittman, D., Eagle, R. A., Neelin, J. D., Mitchell, J. L., & Beaufort, L. (2014, Mar). Modern and glacial tropical snowlines controlled by sea surface temperature and atmospheric mixing. *Nature Geoscience*, *7*(3), 205–209. doi: 10.1038/ngeo2082

UCAR. (n.d.). *2. CLM Technical Note — ctsm release-clm5.0 documentation.* Retrieved from `https://escomp.github.io/ctsm-docs/versions/release-clm5.0/html/tech_note/index.html`

Van Tricht, K., Lhermitte, S., Gorodetskaya, I. V., & van Lipzig, N. P. M. (2016). Improving satellite-retrieved surface radiative fluxes in polar regions using a smart sampling approach. *The Cryosphere*, *10*(5), 2379–2397. Retrieved from `https://tc.copernicus.org/articles/10/2379/2016/` doi: 10.5194/tc-10-2379-2016

Vizcaíno, M., Lipscomb, W. H., Sacks, W. J., & van den Broeke, M. (2014). Greenland Surface Mass Balance as Simulated by the Community Earth System Model. Part II: Twenty-First-Century Changes. *Journal of Climate*, *27*(1), 215 - 226. Retrieved from `https://journals.ametsoc.org/view/journals/clim/27/1/jcli-d-12-00588.1.xml` doi: 10.1175/JCLI-D-12-00588.1

Vuille, M., Francou, B., Wagnon, P., Juen, I., Kaser, G., Mark, B. G., & Bradley, R. S. (2008). Climate change and tropical Andean glaciers: Past, present and future. *Earth-Science Reviews*, *89*(3), 79-96. Retrieved from `https://www.sciencedirect.com/science/article/pii/S0012825208000408` doi: https://doi.org/10.1016/j.earscirev.2008.04.002

Wagnon, P., Lafaysse, M., Lejeune, Y., Maisincho, L., Rojas, M., & Chazarin, J. P. (2009). Understanding and modeling the physical processes that govern the melting of snow cover in a tropical mountain environment in Ecuador. *Journal of Geophysical Research: Atmospheres*, *114*(D19). Retrieved from `https://agupubs.onlinelibrary.wiley.com/doi/abs/10.1029/2009JD012292` doi: https://doi.org/10.1029/2009JD012292

WMO. (1957). Meteorology — a three dimensional science: Second session of the commission for aerology. *WMO Bulletin*, *4*(4), 134–138.